Advancing non-equilibrium ARPES experiments by a 9.3 eV coherent ultrafast photon source

F. Cilento [a,b,*], A. Crepaldi [a], G. Manzoni [c], A. Sterzi [c], M. Zacchigna [b], Ph. Bugnon [d], H. Berger [d], F. Parmigiani [a,c,e]

[a] Elettra – Sincrotrone Trieste S.C.p.A., Strada Statale 14, km 163.5, Trieste 34149, Italy [b] C.N.R. – I.O.M., Strada Statale 14, km 163.5, Trieste 34149, Italy
[c] Universitá degli Studi di Trieste, Via A. Valerio 2, Trieste 34127, Italy
[d] Institute of Condensed Matter Physics, Ecole Polytechnique Fédérale de Lausanne (EPFL), CH-1015 Lausanne, Switzerland [e] International Faculty, University of Köln, 50937 Köln, Germany

a b s t r a c t

The quest for investigating the non-equilibrium dynamics of the band structure of strongly-correlated materials over their entire Brillouin zone is a primary objective. However, the actual ultrafast UV light sources are not suitable for addressing several critical questions in the field. Here we report on a novel light source generating sub-250 fs, 9.3 eV photon energy light pulses at 250 kHz repetition rate, obtained via third-harmonic generation in Xe of frequency-doubled 50 fs laser pulses at 1.55 eV. By reporting the measured band dispersion of a Cu(111) crystal and the non-equilibrium dynamics of the Bi_2Se_3 topological insulator, we prove that this source is suitable for studying the non-equilibrium dynamics of the entire Fermi surface of several complex materials, with high signal statistics and limited space-charge effect.

1. Introduction

Time and angle-resolved photoelectron spectroscopy (TR-ARPES) is a stroboscopic technique based on two synchronized ultrashort optical laser pulses.

In this last decade, TR-ARPES has proved to be of paramount importance for studying the out-of-equilibrium electronic struc-ture of novel materials [1–3] such as topological insulators (TIs) [4–8], graphene [9–12], charge-density-wave materials [13,14] and copper- [15–18] and iron-based [19,20] high temperature super-conductors.

Despite many efforts aimed both to develop the laser technol-ogy and the photoelectron detection, ARPES experiments based on ultrashort laser pulses still have to face problems related to the limited energy and momentum resolution. Actually, produc-ing ultrashort laser pulses with a photon energy suitable to access the entire Brillouin Zone of most materials remains a challeng-ing task, if the energy resolution has to be preserved. This fact leaves pending many important questions in the field of strongly correlated materials. For example, to address topical problems such as the nodal-antinodal dichotomy in cuprate superconductors or the role of the multiband structure of iron-based superconduc-tors, it is mandatory to measure with high energy, momentum and time resolutions the out-of-equilibrium dynamics of the electronic states at the edges of the Brillouin zone (BZ), typically located at a momentum $k \sim 0.85\ A^{-1}$.

Nowadays, these studies are partially precluded to TR-ARPES, since the maximal photon energy for actual TR-ARPES setups exploiting high repetition rate (250–1000 kHz) laser sources is lim-ited to ~6 eV [21,22], and only electronic states at $k_{//}$ smaller than $\sim 0.6\ A^{-1}$ can be probed. Conversely, photons produced by high-harmonic-generation (HHG) of ultrashort laser pulses [23] allow to map the entire BZ of any material. However, the ultimate energy resolution is intrinsically limited to several tens of meV [23] by the bandwidth of the harmonic pulses. Furthermore, the signal statis-tics is relatively poor because of the low repetition rate (typically few kHz) of the laser source, imposed by the high power density (of the order $10^{14}\ W/cm^2$) required to generate these light pulses.

Hence the quest for an ultrafast light source operating at a rep-etition rate exceeding ~100 kHz, delivering photons suitable for covering the entire BZ of most materials and having a bandwidth of ~20–30 meV, is compelling. Recent out-of-equilibrium TR-ARPES studies performed at 6.2 eV probe energy indeed demonstrated

* Corresponding author at: Elettra – Sincrotrone Trieste S.C.p.A., Strada Statale 14, km 163.5, Trieste 34149, Italy. Tel.: +39 0403758461.
E-mail address: federico.cilento@elettra.eu (F. Cilento).

the importance of ultrahigh energy and momentum resolutions (of the order E ≈ 20 meV and k// ≈ 0.003 A^{-1} [24,25] respectively), along with a high signal statistics, for the study of strongly-correlated materials.

Here we report on the development and commissioning of a coherent light source producing vacuum ultraviolet (VUV) 9.3 eV photons at 250 kHz repetition rate and characterized by a pulse length of ~240 fs and an estimated bandwidth of ~35 meV. Our optical setup exploits the third-harmonic generation (THG) process in Xe gas of the second harmonics of a 250 kHz Ti:Sapphire regen-erative amplifier producing ~50 fs laser pulses at 1.55 eV (800 nm) with an energy per pulse in the low- J regime.

The photon energy provided by this source allows to access elec-tronic states lying up to ~1 A^{-1}. At the same time, the accessible binding energy range allows to study the non-equilibrium dynam-ics of electronic states lying up to ~2.5 eV below the Fermi energy. The performances of this source have been tested in ARPES and TR-ARPES reference experiments. The outcome of these experi-ments demonstrate that this source advances those actually used for TR-ARPES experiments, meanwhile joining their advantages. In particular, the 250 kHz repetition rate ensures high statistics and almost space-charge-free experiments.

2. Motivation

An important achievement that would advance our under-standing of the physics of strongly-correlated materials arises from the possibility to completely characterize the nature and strength of the electronic correlations. An orbital-selective [26] or momentum-space-selective [27] degree of electronic correlation could be directly revealed by TR-ARPES experiments by measur-ing the temporal evolution of the quasi-particle scattering rate, provided that the out-of-equilibrium mapping of the electronic states over the entire BZ of these materials is possible. The results of such experiments will be of paramount importance in order to verify the 'selective Mottness' theory [26], that reconciles the unconventional properties of both the iron- and the copper-based high-temperature superconductors.

As an example, Fig. 1 reports the calculated Fermi Surface in the first BZ of the Bi2212 cuprate superconductor, obtained by

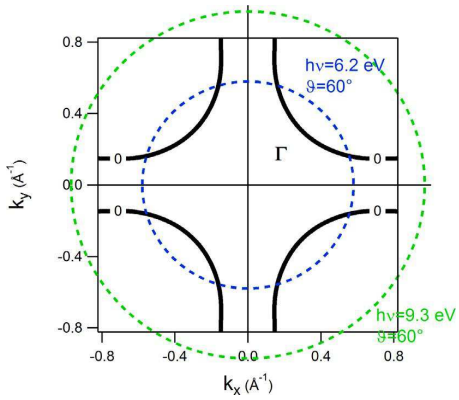

Fig. 1. The Fermi surface of Bi2212 is reported as black lines representing the Fermi arcs. The dashed blue circle encloses the momentum space region that can be accessed using 6.2 eV photons (see text). Dashed green circle represents the situ-ation when using 9.3 eV photons. These curves has been drawn by assuming a work function = 4.5 eV and a maximum emission angle = 60°. 9.3 eV photons deter-mine a maximum accessible crystal momentum ~70% larger than at 6.2 eV, allowing to access the entire Fermi surface of cuprates. (For interpretation of the references to color in this figure legend, the reader is referred to the web version of this article.)

using a tight-binding approach [28]. Two dashed circles enclose the momentum regions that can be mapped by using 6.2 eV photons (blue) and 9.3 eV photons (green).

In particular, at 6.2 eV probe energy the study of the antinodal region is precluded, whereas at 9.3 eV, the entire Fermi surface of the Bi2212 and other cuprates can be accessed.

A problem arising when studying electronic phases that can be easily vaporized by a light pulse, like the superconducting state [29], is that the excitation of the material must be performed at a very low fluence (~20 J/cm^2). Hence, a high repetition rate of the laser source is mandatory to provide a signal-to noise ratio high enough to reveal low intensity out-of-equilibrium signals. Under these operating conditions the space charge effect [30–35] is sig-nificantly reduced, and high energy and momentum resolutions are preserved. The ideal case is realized with ~1 photoelectron-per-pulse, an experimental condition that is easily obtained with setups operating at a repetition rate in the 250–1000 kHz range, while challenging at the 1–10 kHz repetition rate of most of the HHG-based TR-ARPES setups.

3. The VUV Source

3.1. Optical and UHV apparatus

Fig. 2 shows the schematic of the TR-ARPES system, including the laser source, the optical setup for 9.3 eV generation and a sketch of the UHV ARPES chamber. The source is based on the THG in Xe gas of the second harmonics at 3.1 eV of a 250 kHz Ti:Sapphire regener-ative amplifier delivering an energy per pulse in the low- J regime. In the figure the color-coding for the photon-energies involved in the setup is defined. The laser fundamental beam at 1.55 eV is indi-cated in red, its second harmonic beam at 3.1 eV in blue, while the
9.3 eV beam in light-blue.

The laser source produces ~50 fs FWHM (full-width at half max-imum) pulses at = 800 nm (ω0 = 1.55 eV), with a pulse-energy of ~6 J (1.5 W average power) when operating at 250 kHz. A frac-tion of the laser output (<10%) is used as the pump beam, and the pump-probe delay is controlled by a motorized translation stage. The pump beam is focused on the sample with a 750 mm focal length lens, and it has a full-width-half-maximum (FWHM) spot size of 500 ± 20 m. The probe beam is frequency-doubled in a 0.5 mm thick ˇ-barium borate (BBO) non-linear crystal, cut at an angle of 29.2°. Using a 250 mm focal length lens to focus the radia-tion on the BBO crystal, we obtain a conversion efficiency of ~40%, corresponding to 400 mW power (1.6 J/pulse) at 3.1 eV. This beam, with a FWHM diameter D = 5 mm, is used for third harmonic gen-eration in gas. It is focused by a 36 mm focal length lens in the gas

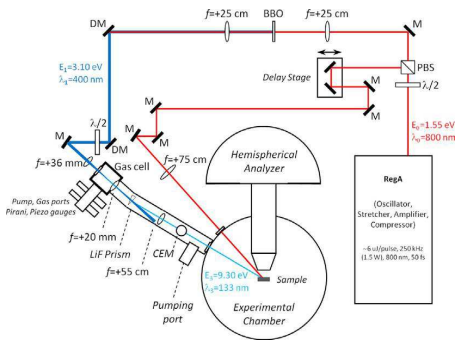

Fig. 2. The block diagram of the experimental apparatus with the 9.3 eV source is sketched. M: mirror; DM: dichroic mirror; PBS: polarizing beamsplitter cube.

cell, with a spot size at the focus position of 10 m FWHM. The con-focal parameter in this geometry is ~400 m. The resulting power density at the waist position, available for harmonic generation, is of the order 1.5 × 10^{13} W/cm^2 .

The system for third-harmonic generation in Xe is based on a gas cell and a tube chamber, where the 9.3 eV harmonic beam is split from the 3.1 eV beam by a prism and is then focused on the sample in the UHV ARPES chamber. The limited energy-per-pulse avail-able requires a tight-focusing geometry for the seeding radiation, and allows for a compact design of the source. This tight focusing geometry is defined as the regime for which the confocal parameter b of the focused Gaussian beam is much smaller than the length L of the active medium, i.e., b L. L is typically the length of the gas cell, as it is the case of our experiment, or the size of the gas-jet. The opposite regime, b L, is routinely used in HHG setups seeded by low (~kHz) repetition rate laser sources, where loosely focused beams and gas-jets are used.

The gas cell is constituted by a 34 mm CF16 UHV cube. The entrance window is a 1.5 mm thick fused-silica plate, while the exit window is a MgF_2 20 mm focal length lens, with central thickness equal to 2.5 mm. One optics is used to both separate the two cham-bers and collimate the harmonic beam. The gas-cell is equipped with an evacuation port, a valve for introducing the gas and two pressure gauges. A Pirani sensor is used for measuring the vac-uum level after evacuation and a piezo-based sensor is used for measuring the Xe pressure. A precise pressure tuning in the gas cell is obtained by a limiting valve controlling the gas flow. Once the optimal pressure is set in the gas cell, operation of the source can proceed without requiring to replace the gas. The second vac-uum chamber is constituted by an angled tube in which a LiF prism with 20° apex angle is mounted, for separating the 3.1 eV seed beam from its third harmonics at 9.3 eV. The prism is mounted on a motorized mount, ensuring a reproducible and remote-controlled operation. The angled tube was designed for ensuring that the trajectory of the 9.3 eV refracted beam matches the minimum dis-persion angle of the LiF prism, equal to 11.5° . After separation, the harmonic radiation is focused on the sample with a MgF_2 550 mm focal length lens, to a spot size of 400 ± 50 m. The tube chamber is also equipped with a channeltron electron multiplier (CEM) detec-tor, mounted on a translation stage, for measuring the harmonic signal. Finally, the tube chamber ends with a double-side, 3 mm thick CF40 MgF_2 viewport, that physically separates the harmon-ics source from the UHV ARPES chamber. This window ensures a transmittivity of ~50% at 9.3 eV. The output signal from the CEM is amplified by a voltage-to-current converter with a 10^5 V/A ratio and subsequently acquired via a fast digitizer. The conversion from the acquired voltage to the number of photons per second takes into account the gain of the CEM (~10^6 at 1600 V, [36]) and its quantum efficiency (~0.01 at 9.3 eV, [37]), and results of the order of ~10^9 V/A or ~1.6 × 10^6 photons/(V s). These estimations are affected by a ±30% uncertainty arising from a possible inaccuracy of the val-ues of CEM gain and quantum efficiency. Finally, the polarization of the 9.3 eV beam can be easily tuned between linear-vertical (s) and linear-horizontal (p) by simply rotating a /2 waveplate placed on the second-harmonic beam, without affecting the VUV beam transmission to the sample.

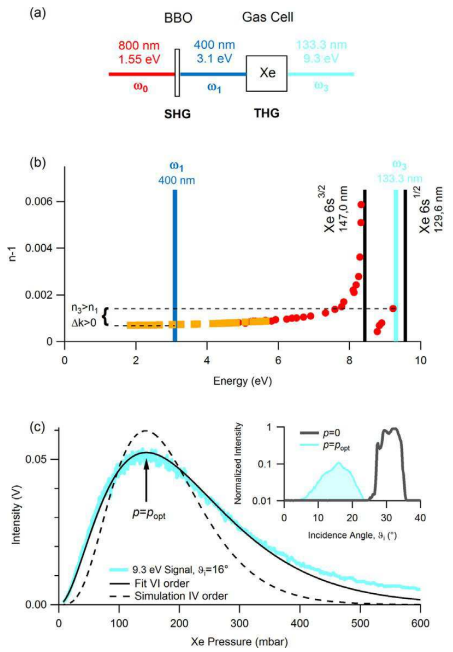

Fig. 3. (a) Block diagram of the optical setup. The laser fundamental of the Ti:Sapphire laser source (1.55 eV, red) is frequency doubled in a BBO crystal (SHG, 3.1 eV, blue), and subsequently frequency tripled in a Xe-filled gas cell (THG, 9.3 eV, light-blue). (b) The refractive index n – 1 of Xe is reported in the energy range of the resonance lines, at 147.0 nm and 129.6 nm, relevant to the case of THG at 9.3 eV. Data reported as red dots are taken from [54], yellow squares from [55]. Xenon gives a positive wavevector mismatch in the case of THG of 3.1 eV pulses. (c) Pressure tun-ing curve reporting the harmonic intensity as a function of Xe pressure. The curve is obtained for an incidence angle $_i$ = 16° on the LiF prism, corresponding to the condition of minimum deviation for the VUV beam. The fit to the measured pres-sure tuning curve of the phase-matching expression in the case of a six-wave mixing process is reported as a solid black line. Dashed black line is a simulation for the case of a four-wave mixing process. In both cases, the confocal parameter is b = 0.4 mm. In the inset, the normalized intensity resulting from the scan of the prism angle is reported, for p = 0 and p = p_{opt} . The 3rd harmonic signal is evidenced in light-blue. The peak at ~30° is due to the 3.1 eV beam, reported in gray. (For interpretation of the references to color in this figure legend, the reader is referred to the web version of this article.)

3.2. Third harmonic generation in gases

Fig. 3(a) schematizes the non-linear interactions exploited for 6th harmonic generation (6HG). Generation of laser pulses in the VUV range via non-linear mixing processes requires exploiting gases as non-linear media, since for photon energies larger than ~7 eV, there are no crystals that can ensure a suitable phase match-ing and transparency [38]. In the past years the modeling of the phase-matching conditions in gaseous media has been matter of several studies [39–44], and experiments where these generation schemes have been applied to spectroscopies have been reported [45–51].

In gases, having null even-order susceptibilities, the third-order susceptibility can be significant, especially in the vicinity of sharp resonance absorption lines. When the phase-matching condition k = 0 is fulfilled, the non-linear conversion efficiencies can be as high as 10^{-2} [52,53] for THG.

In the case of THG, the phase-mismatchk between the harmonic radiation and the seeding radiation writes k = k_3 – 3k_1 = 6 / $_1$ (n_3 – n_1), n_j being the refractive index. Phase matching k = 0 can be obtained by proper gas mixtures, by gas pressure tuning or by selecting a couple of wavelengths such that k = 0. This last option is accessible by working across resonance lines of gases.

Harmonics generation seeded by laser pulses of moderate inten-sity requires to tightly focus the laser beam for achieving a power density exceeding 10^{12} W/cm^2 [38,56]. By focusing a Gaussian beam a phase shift k_{geom} , known as Gouy term, is introduced because of a slip in phase between the seed and the harmonic radiation [38,39], as the beam travels through the focal region. For sizeable harmonic production, this net phase-mismatch must

be compensated by a wavevector mismatch coming from the dis-persion of the nonlinear medium, indicated as k_{gas} , in such a way the total wavevector mismatch $k_{tot} \equiv k_{geom} + k_{gas}$ is zero.

It is worth noting that the geometry-induced phase slip modi-fies the ideal phase matching condition k = k_{gas} = 0 into the less stringent $k_{tot} = k_{geom} + k_{gas}$ condition. This is advantageous, since perfect phase matching k_{gas} = 0 can only be obtained for rare combinations of seed and harmonic frequencies depending on the dispersion of the medium. Conversely, the requirement k_{tot} = 0 with $k_{gas} \neq 0$ allows exploiting gas mixtures or gas pressure tun-ing for tailoring the gas refractive index and compensating the geometry-induced phase shift.

The value and sign of the geometry-related phase shift k_{geom} depends on both the focusing geometry and the non-linear mix-ing process under consideration [39]. The simplest process leading to THG is a degenerate four-wave mixing, a third-order process described by $\omega^{iv} = \omega^{i} + \omega^{ii} + \omega^{iii}$, with $\omega^{i} = \omega^{ii} = \omega^{iii}$. In this frame, the harmonic intensity, I, follows the form $I \propto (b\, k_{gas})^{4} \exp(b\, k_{gas})$ in the limit b L and $I \propto (b\, k_{gas})^{2} \exp(b\, k_{gas})$ in the limit b L (b is the confocal parameter of the focused seeding radiation and L the length of the active medium). As a consequence, the opti-mal phase mismatch is obtained for $k_{gas} = -4/b$ in the limit b L and for $k_{gas} = -2/b$ in the limit b L. These results come from the solution of the phase matching integral, as reported in [38,39]. Hence, THG as a result of a degenerate four-wave mixing process in the tight focusing geometry is only possible for a negative phase mismatch, i.e., $k_{gas} < 0$, corresponding to the negative-dispersion regime, whereas no THG is allowed in positive dispersion regime [40].

Xenon, as well as other inert gases, displays a positive phase mis-match between ω_1 = 3.1 eV and its third harmonics at ω_3 = 9.3 eV [54,55,57], as shown in Fig. 3(b). For these energies, k_{gas} is posi-tive and its magnitude can be tuned by adjusting the gas pressure, although its sign cannot be changed. Here we show that THG is also possible in this condition. Since the degenerate four-wave mix-ing interaction $\omega^{iv} = 3\omega^{i}$ ($\omega^{iv} = \omega_3$, $\omega^{i} = \omega_1$) cannot lead to THG with $k_{gas} > 0$, harmonic generation arises from a mechanism involving a higher-order non-linearity. In particular, as reported in [40], the interaction leading to THG is a six wave mixing phenomenon (a fifth-order process), described as $\omega^{iv} = 4\omega^{i} - \omega^{i}$ ($\omega^{iv} = \omega_3$, $\omega^{i} = \omega_1$), which is instead allowed for positive dispersion of the gas. The har-monic intensity I in the case $k_{gas} > 0$ and in the tight-focusing limit b L is given by $I \propto \exp(-b\, k_{gas})$ [40].

Xe was selected because it allows high conversion efficiency (it has the lowest ionization energy among inert gases, thus it is more polarizable yielding to a large non-linear coefficient) and because its resonances lye far from both the seed and harmonic energy, thus avoiding resonant effects [41].

The optimization of the harmonic production is performed via gas pressure tuning. The optimal condition is obtained when the geometrical phase mismatch k_{geom} is compensated by the phase mismatch due to the medium, $k_{gas} > 0$, that depends linearly on the gas pressure p as: $k_{gas}(p) = 6\,/\,_1\,(n_3(p) - n_1(p))$, where $n_j(p) = 1 + d_j\,(p - p_0)/p_0$, $_1$ being the fundamental wavelength in vacuum, n_j the refraction indexes, d_j a coefficient independent on pressure and p_0 a reference pressure. Hence, pressure tuning allows to obtain the optimal phase matching condition k_{tot} = 0 for the seed beam at 3.1 eV and its third harmonics at 9.3 eV, for maximal harmonic production. Fig. 1(c) shows the generated 9.3 eV beam intensity, detected by the CEM detector, as a function of Xe pressure in the gas cell.

The inset of Fig. 3(c) shows two clearly resolved features assigned to the 3.1 eV seeding beam and the 9.3 eV harmonics beam, detected upon scanning of the incidence angle of the dis-persing prism. The width of the peaks does not reflect their actual spectral bandwidth. It is given by the fact that the angle of a beam of finite size is scanned across the active area of the detector, which is 10 mm wide in our experiment.

The angle of minimum deviation of the 9.3 eV beam is found to be in good agreement (within $\pm 0.5^{\circ}$) with the calculated value of 11.5° , determined by simulating the dispersion angle of a LiF prism with apex angle equal to 20° and refractive index n = 1.569 [58] at 133 nm. This minimum dispersion condition is obtained for an incidence angle on the prism equal to $16 \pm 0.5^{\circ}$, at which the maximum of the 9.3 eV beam peak is recorded.

The optimal phase matching condition is found by tuning Xe pressure till the maximum harmonic generation is recorded. In our setup this is obtained at $p_{opt} = 145 \pm 10$ mbar. At this pressure, the measured voltage is ~50 mV (see Fig. 3(c)), corresponding to a flux of $\sim 8 \times 10^{8}$ photons/s. The generation efficiency, considering the 3.1 eV beam power of 400 mW, is slightly larger than 10^{-9} . Consid-ering an overall transmittivity T ~ 50 %, a flux of $\sim 4 \times 10^{8}$ photons/s at the sample position is estimated. It is worth noting that optimiza-tion of the conversion occurs at progressively higher pressures as the beam is focused more tightly (p_{opt} increases as the confocal parameter b is reduced), hence harmonic production increases as the beam is focused more tightly.

For interpreting the pressure tuning curve reported in Fig. 3(c), it is important to consider that, when the optimization of the har-monic intensity is performed by varying the gas pressure, both the gas density N and the phase mismatch k are affected, and the phase matching integrals must be modified [39]. In particular, the quantity that maximizes the harmonic production is obtained by multiplying the square of the phase-matching integrals by $(b\, k)^{2}$. Thus, in the limit b L, the functional form that describes THG via the 5th order process $\omega^{iv} = 4\omega^{i} - \omega^{i}$ ($\omega^{iv} = \omega_3$, $\omega^{i} = \omega_1$)

is $(b\, k_{gas})^{2} \exp(-b\, k_{gas})$, for $k_{gas} > 0$, while the one expected for THG via the 3rd order process $\omega^{iv} = 3\omega^{i}$ ($\omega^{iv} = \omega_3$, $\omega^{i} = \omega_1$) is $(b\ \ k_{gas})^{4} \exp(b\ \ k_{gas})$, for $k_{gas} < 0$.

The fitting of the expression for the 5th order process to the experimental data shows excellent agreement between the data and the phase-matching model (see Fig. 3(c)). Only at the higher gas pressures, where competing phenomena are likely to be at play, a small departure is observed. This fact confirms that the non-linear interaction leading to THG is of fifth order, i.e., $\omega^{iv} = 4\omega^{i} - \omega^{i}$. The maximum conversion efficiency is obtained for a pressure corresponding to the condition k_{gas} = +2/b. On the contrary, the simulation of the curve that would have been obtained for a third-order degenerate sum-frequency mixing (represented by the dashed line in Fig. 1(c)) indicates that this process (beyond the wrong sign of the dispersion of the medium) cannot be responsible for the observed harmonic production.

4. Results and discussion

To prove that this source can open new important routes it has been tested in ARPES and TR-ARPES experiments using a Cu(111) single crystal and the TI $Bi_2 Se_3$. Cu(111) presents a non-dispersing d-band and dispersing 4 sp bands both within the accessible energy and momentum range of the present setup [59], and thus consti-tutes an ideal benchmark. Likewise, TIs are known for their peculiar electronic structure, consisting in a bulk insulating or semiconduct-ing band gap and in a spin polarized metallic surface state [60]. They have recently attracted a large attention as promising materials for realizing opto-spintronic devices. Extensive information about their electronic structure studied by ARPES [61–63] and TR-ARPES [4–8] is available in the literature. In particular, TIs exhibit a large variation of the occupation of both the bulk and of the topologically protected surface state, when excited by ultrashort infrared laser pulses [4].

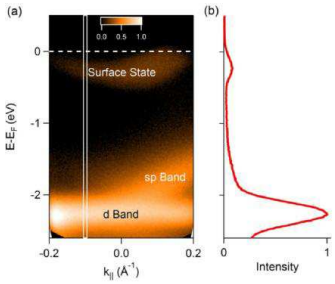

Fig. 4. (a) ARPES intensity map acquired on a Cu(111) single crystal at T = 120 K. The surface state, the flat d band the sp band are simultaneously resolved. The color cod-ing is indicated by the colorscale. (b) The EDC extracted at $k_{//} = -0.1$ Å^{-1} is reported. The intensity has been integrated over a 0.01 Å^{-1} momentum window, as indicated by the solid white box drawn in (a). (For interpretation of the references to color in this figure legend, the reader is referred to the web version of this article.)

Fig. 4(a) reports the ARPES band dispersion of the Cu(111) single crystal, as measured at T = 120 K. The spectrum has been acquired on a clean surface showing an ordered 1 × 1 reconstruc-tion, as observed by low energy electron diffraction (LEED). The main relevant band dispersion features, namely the flat d-bands, lying ~2 eV below the Fermi level, and the Shockeley surface states, are clearly detected. An additional dispersing band, orig-inated from hybridized sp states, is also detected. These results are in good agreement with the literature [64]. Fig. 4(b) shows an energy-distribution-curve (EDC) integrated over a 0.01 Å^{-1} win-dow centered at $k_{//} = 0.1$ Å^{-1}, as indicted by the white box in Fig. 4(a). We stress the capability of the setup developed to access electronic states lying ~2 eV below the Fermi level, that is precluded to ARPES at ~6 eV photon energy.

Fig. 5(a) shows the ARPES data from a high quality TI Bi_2Se_3 single crystal measured at T = 120 K. Both the topological surface state and the conduction band are resolved. Fig. 5(b) shows an EDC extracted at $k_{//} = 0$ across the Fermi level, integrated over a 0.02 Å^{-1} window (solid white box in Fig. 5(a)). Fitting a function given by the product of a Lorentzian peak (accounting for the con-duction band) and a Fermi–Dirac function at T = 120 K, convoluted with a Gaussian function accounting for the experimental energy resolution, to the EDC, we are able to extract the overall energy reso-lution achieved with this setup. The FWHM of the Gaussian resulted dE = 100 ± 10 meV, overall determined by the electron analyzer pass energy (10 eV) and slit aperture (0.5 mm), both set for achieving a reasonable acquisition time (~10) with the moderate flux available at present. With the data reported in Fig. 5(a) we prove the capa-bility of our setup to resolve the topological surface state from the conduction band of Bi_2Se_3 , a performance which is not achieved with current HHG sources [8].

In order to estimate the overall temporal resolution of this setup, a TR-ARPES experiment on the TI Bi_2Se_3 has been performed. Fig. 5(c) shows the temporal dynamics of the ARPES intensity, inte-grated over the area delimited by the white box drawn in the inset. For maximizing the statistics, the slit width of the analyzer was set to 2 mm. The dynamics, induced by an absorbed pump fluence of 100 ± 10 J/cm^2 at 1.55 eV, has been recorded over a 6.6 ps delay range. In order to extract the ultimate temporal reso-lution of the setup, we fit a single-exponentially decaying function convoluted with a Gaussian function accounting for the temporal cross-correlation (dt) to the time trace of Fig. 5(c). In performing the fitting procedure, we also take into account a 350 fs rise time that is needed to fit equivalent time traces acquired with the conventional 6.2 eV setup [4], that presents a cross-correlation of 250 ± 10 fs, as measured with an optical cross correlation technique. The result of the fitting procedure yields = 2.8 ps for the exponential decay,

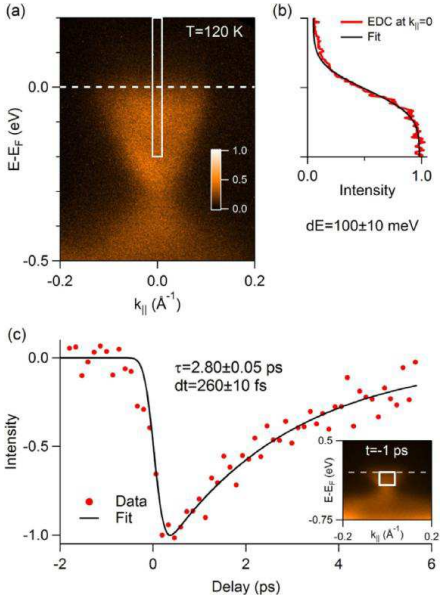

Fig. 5. (a) ARPES intensity map acquired on the TI Bi_2Se_3 at T = 120 K. The intensity is indicated by the colorscale. The Fermi level E_F is at $E_{kin} = 4.69 \pm 0.01$ eV. (b) The EDC at $k_{//} = 0$, integrated over a 0.02 Å^{-1} window (as shown by the white box in (a)) is reported (red line). The fitting of a Fermi–Dirac function at T = 120 K convoluted with the experimental resolution dE to the EDC (black line) gives an energy resolution dE = 100 ± 10 meV. The ARPES intensity of the conduction band (red dots) is reported as a function of pump-probe delay t, revealing the pump-induced depletion of the band. The result of the fitting procedure (see main text) gives a relaxation time = 2.80 ± 0.05 ps and an experimental time resolution dt = 260 ± 10 fs (FWHM), and is reported as a solid black line. The inset shows the ARPES intensity map acquired at the pump-probe delay t = −1 ps. The white box indicates the area on which the intensity reported in panel (c) was integrated. (For interpretation of the references to color in this figure legend, the reader is referred to the web version of this article.)

in excellent agreement with previous results [4–7], and dt = 260 fs (FWHM) for the cross-correlation, a result which is mainly due to the chirp acquired by the VUV beam as it traverses the optical elements of the setup.

After deconvolution of the pump pulse FWHM (70 fs), we obtain a pulse FWHM of 240 ± 10 fs for the 9.3 eV pulse at the sample position. This value represents a novel experimental determina-tion of the pulse duration of THG obtained in the positive dispersion regime, by seeding the generation process with femtosecond laser pulses. This result seems to confirm the predictions reported in [40], suggesting that an ultrashort VUV pulse can be generated in the case of positive dispersion of the gas with a six-wave mixing process.

Finally, we provide an estimate of the energy bandwidth of the VUV pulse. This is obtained starting from the knowledge of the pulse temporal FWHM at the sample position, $_{sample}$ = 240 ± 10 fs, taking into account the temporal chirp acquired by the VUV beam as it travels from the source to the sample. Under the reasonable assumption that the chirp of the VUV pulse is only acquired because of the propagation of the beam through optical elements, it is pos-sible to calculate the VUV pulse duration at the source, $_{source}$, through the relation $_{sample} = _{source}^{-1} / (\sqrt{_{source}^{4} + 16(\ln 2)^2 GDD^2})$, describing the propagation of Gaussian beams in dispersive media.

The 9.3 eV beam travels through four optical elements, contributing with overall ~7.5 mm MgF_2 glass and ~1 mm LiF glass. At 9.3 eV, the Group Velocity Dispersion (GVD) is equal to +517.29 fs^2 /mm for MgF_2 glass [65] and +413.68 fs^2 /mm for LiF glass [66]. This means the total Group Delay Dispersion (GDD) is 4293 fs^2 . Hence,

we obtain the value $_{source}$ = 50 ± 5 fs for the VUV beam at the source position. This implies a 35 ± 3 meV FWHM bandwidth at 9.3 eV. This value sets the ultimate energy resolution that could be achieved in ARPES measurements, and also indicates that by reducing the num-ber of optical elements in the setup, the temporal resolution can be further improved.

5. Summary and perspectives

In summary, we reported on the development and character-ization of an ultrafast 9.3 eV VUV laser light source that can be driven by high repetition rate Ti:Sapphire regenerative lasers. With this source, the momentum mapping capability of TR-ARPES setups reaches ~1 A^{-1}, allowing to measure the non-equilibrium dynam-ics of the electronic states over the entire BZ of most materials, with a temporal resolution of the order ~240 fs. With our exper-iment, we proved that THG in inert gas is a suitable method for producing ultrashort VUV light pulses to be used in TR-ARPES experiments. At the same time, this source overcomes the prob-lems of a low statistics intrinsic of TR-ARPES setups based on HHG sources, while allowing for significantly higher energy and momen-tum resolutions. The conversion efficiency for THG in Xe is of the order ~10^{-9}, because the non-linear process leading to THG is a six-wave mixing [48] obtained in the positive-dispersion regime, as we proved by modeling the measured pressure tuning curve. Despite the moderate conversion efficiency of this non-linear process, the generated flux is enough for performing TR-ARPES experiments in a reasonable amount of time. The present performances are going to significantly improve by using laser sources providing a tunable photon energy with a multi- J energy-per-pulse, for entering the negative-dispersion regime [67] thus allowing THG from a four-wave-mixing interaction. This will result in a three-to-four orders of magnitude boost in the harmonic production.

Only very recently many novel setups for achieving HHG at high repetition rate [68–82] have been presented. Development of these novel sources have been made possible by the recent progresses of laser technology. In particular, high-power laser sources (with an average power that can be in excess of ~100 W) working at high repetition rate (50–600 kHz) are exploited. However, common to most of these sources is an intrinsic harmonics bandwidth of the order 50–100 meV, thus limiting the overall energy resolution in ARPES experiments.

Considering the results of the experiments reported, the 9.3 eV ultrafast VUV source opens the way to the investigation, with high statistics and high energy-momentum resolutions, of the non-equilibrium electron dynamics over the entire BZ of materials with a complex Fermi surface or a multiband structure.

This work was funded by the FERMI project of Elettra-Sincrotrone Trieste, partially supported by the Ministry of University and Research (Grant Nos. FIRBRBAP045JF2 and FIRBR-BAP06AWK3).

References

[1] U. Bovensiepen, Dynamics at Solid State Surfaces and Interfaces, Wiley, 2012.
[2] S. Hüfner, Photoelectron Spectroscopy: Principles and Applications, Springer, 2010.

[3] A. Damascelli, Z. Hussain, Z.-X. Shen, Rev. Mod. Phys. 75 (2003) 473.
[4] A. Crepaldi, B. Ressel, F. Cilento, M. Zacchigna, C. Grazioli, H. Berger, P. Bugnon, K. Kern, M. Grioni, F. Parmigiani, Phys. Rev. B 86 (2012) 205133.
[5] J.A. Sobota, S. Yang, J.G. Analytis, Y.L. Chen, I.R. Fisher, P.S. Kirchmann, Z.-X. Shen, Phys. Rev. Lett. 108 (2012) 117403.
[6] M. Hajlaoui, E. Papalazarou, J. Mauchain, G. Lantz, N. Moisan, D. Boschetto, Z. Jiang, I. Miotkowski, Y.P. Chen, A. Taleb-Ibrahimi, L. Perfetti, et al., Nano Lett. 12 (2012) 3532.

[7] Y.H. Wang, D. Hsieh, E.J. Sie, H. Steinberg, D.R. Gardner, Y.S. Lee, P. Jarillo-Herrero, N. Gedik, Phys. Rev. Lett. 109 (2012) 127401.
[8] A. Crepaldi, F. Cilento, B. Ressel, C. Cacho, J.C. Johannsen, M. Zacchigna, H. Berger, P. Bugnon, C. Grazioli, I.C.E. Turcu, et al., Phys. Rev. B 88 (2013), 121404(R).
[9] J.C. Johannsen, S. Ulstrup, F. Cilento, A. Crepaldi, M. Zacchigna, C. Cacho, I.C.E. Turcu, E. Springate, F. Fromm, et al., Phys. Rev. Lett. 111 (2013) 127403.
[10] S. Ulstrup, J.C. Johannsen, F. Cilento, J.A. Miwa, A. Crepaldi, M. Zacchigna, C. Cacho, R. Chapman, E. Springate, S. Mammadov, et al., Phys. Rev. Lett. 112 (2014) 257401.

[11] I. Gierz, J.C. Petersen, M. Mitrano, C. Cacho, I.C.E. Turcu, E. Springate, A. Stöhr, A. Köhler, U. Starke, A. Cavalleri, Nat. Mater. 12 (2013) 1119.
[12] L. Bignardi, T. Haarlammert, C. Winter, M. Montagnese, P.H.M. van Loosdrecht, E. Voloshina, P. Rudolf, H. Zacharias, Phys. Rev. B 89 (2014) 075405.
[13] L. Perfetti, P.A. Loukakos, M. Lisowski, U. Bovensiepen, H. Berger, S. Biermann, P.S. Cornaglia, A. Georges, M. Wolf, Phys. Rev. Lett. 97 (2006) 067402.
[14] F. Schmitt, P.S. Kirchmann, U. Bovensiepen, R.G. Moore, J.-H. Chu, D.H. Lu, L. Rettig, M. Wolf, I.R. Fisher, Z.-X. Shen, New J. Phys. 13 (2011) 063022.
[15] L. Perfetti, P.A. Loukakos, M. Lisowski, U. Bovensiepen, H. Eisaki, M. Wolf, Phys. Rev. Lett. 99 (2007) 197001.
[16] R. Cortés, L. Rettig, Y. Yoshida, H. Eisaki, M. Wolf, U. Bovensiepen, Phys. Rev. Lett. 107 (2011) 097002.
[17] W. Zhang, C. Hwang, C.L. Smallwood, T.L. Miller, G. Affeldt, K. Kurashima, C. Jozwiak, H. Eisaki, T. Adachi, Y. Koike, et al., Nat. Commun. 5 (2014) 4959.
[18] C.L. Smallwood, W. Zhang, T.L. Miller, C. Jozwiak, H. Eisaki, D.-H. Lee, A. Lanzara, Phys. Rev. B 89 (2014) 115126.
[19] L. Rettig, R. Cortés, H. Jeevan, P. Gegenwart, T. Wolf, J. Fink, U. Bovensiepen, New J. Phys. 15 (2013) 1367.
[20] I. Avigo, R. Cortés, L. Rettig, S. Thirupathaiah, H. Jeevan, P. Gegenwart, T. Wolf, M. Ligges, M. Wolf, J. Fink, et al., J. Phys.: Condens. Matter 25 (2013) 094003.

[21] J. Faure, J. Mauchain, E. Papalazarou, W. Yan, J. Pinon, M. Marsi, L. Perfetti, Rev. Sci. Instrum. 83 (2012) 123904.
[22] C.L. Smallwood, C. Jozwiak, W. Zhang, A. Lanzara, Rev. Sci. Instrum. 83 (2012) 123904.

[23] F. Frassetto, C. Cacho, C.A. Froud, I.E. Turcu, P. Villoresi, W.A. Bryan, E. Springate, L. Poletto, Opt. Express 19 (2011) 19169.
[24] C.L. Smallwood, J.P. Hinton, C. Jozwiak, W. Zhang, J.D. Koralek, H. Eisaki, D.-H. Lee, J. Orenstein, A. Lanzara, Science 336 (2012) 1137.
[25] J. Graf, C. Jozwiak, C.L. Smallwood, H. Eisaki, R.A. Kaindl, D.-H. Lee, A. Lanzara, Nat. Phys. 7 (2011) 805.
[26] L. de' Medici, G. Giovannetti, M. Capone, Phys. Rev. Lett. 112 (2014) 177001.
[27] F. Cilento, S.D. Conte, G. Coslovich, S. Peli, N. Nembrini, S. Mor, F. Banfi, G. Ferrini, H. Eisaki, M.K. Chan, et al., Nat. Commun. 5 (2014) 4353.
[28] M.R. Norman, Phys. Rev. B 61 (2000) 14751.
[29] C. Giannetti, G. Coslovich, F. Cilento, G. Ferrini, H. Eisaki, N. Kaneko, M. Greven, F. Parmigiani, Phys. Rev. B 79 (2009) 224502.
[30] J. Graf, S. Hellmann, C. Jozwiak, C.L. Smallwood, Z. Hussain, R.A. Kaindl, L. Kipp, K. Rossnagel, A. Lanzara, J. Appl. Phys. 107 (2010) 014912.
[31] S. Hellmann, K. Rossnagel, M. Marczynski-Bühlow, L. Kipp, Phys. Rev. B 79 (2009) 035402.
[32] G. Liu, G. Wang, Y. Zhu, H. Zhang, G. Zhang, X. Wang, Y. Zhou, W. Zhang, H. Liu, L. Zhao, et al., Rev. Sci. Instrum. 79 (2008) 023105.
[33] S. Passlack, S. Mathias, O. Andreyev, D. Mittnacht, M. Aeschlimann, M. Bauera, J. Appl. Phys. 100 (2006) 024912.
[34] X. Zhou, B. Wannberg, W. Yang, V. Brouet, Z. Sun, J. Douglas, D. Dessau, Z. Hussain, Z.-X. Shen, J. Electr. Spectrosc. Relat. Phenom. 142 (2005) 27.
[35] M. Dell'Angela, T. Anniyev, M. Beye, R. Coffee, A. Föhlisch, J. Gladh, S. Kaya, T. Katayama, O. Krupin, A. Nilsson, et al., Struct. Dyn. 2 (2015) 025101.
[36] See http://www.sjuts.com/Quality Gain.html.
[37] See http://www.sjuts.com/Quality efficiencies.html.
[38] J.F. Reintjes, Nonlinear Optical Parametric Processes in Liquids and Gases, Aca-demic Press, 1984.
[39] G.C. Bjorklund, IEEE J. Quantum Electron. 11 (1975) 287.
[40] J. Kutzner, H. Zacharias, Appl. Phys. B 66 (1998) 571.
[41] J. Kutzner, G. Tsilimis, H. Zacharias, Appl. Phys. 80 (2005) 203.
[42] A. Lago, G. Hilber, R. Wallenstein, Phys. Rev. A 36 (1987) 3827.
[43] J. Rothhardt, M. Krebs, S. Hädrich, S. Demmler, J. Limpert, A. Tünnermann, New J. Phys. 16 (2014) 033022.
[44] A. Cabasse, G. Machinet, A. Dubrouil, E. Cormier, E. Constant, Opt. Lett. 37 (2012) 4618.
[45] T. Munakata, T. Masuda, N. Ueno, A. Abdureyim, Y. Sonoda, Surf. Sci. 507 (2002) 434.

[46] T. Munakata, K. Mase, I. Kinoshita, Surf. Sci. 286 (1993) 73.
[47] T. Munakata, E. Ishikawa, I. Kinoshita, T. Kasuya, Rev. Sci. Instrum. 62 (1991) 2572.

[48] K. Kimura, M. Takahashi, K. Okuyama, I. Plazibat, J. Electr. Spectrosc. Relat. Phenom. 51 (1990) 383.
[49] T. Munakata, T. Masuda, N. Ueno, S. Sakaya, T. Sugiyama, N. Takehiro, Y. Sonoda, Surf. Sci. 532 (2003) 1140.
[50] J. Bokor, N.J. Halas, IEEE J. Quantum Electron. 25 (1987) 2550.
[51] M.H. Berntsen, O. Götberg, O. Tjernberg, Rev. Sci. Instrum. 82 (2011) 095113.
[52] R. Hilbig, R. Wallenstein, IEEE J. Quantum Electron. 17 (1981) 1566.
[53] L.J. Zych, J.F. Young, IEEE J. Quantum Electron. 14 (1978) 147.
[54] A. Bideau-Mehu, Y. Guern, R. Abjean, A. Johannin-Gilles, J. Quant. Spectrosc. Radiat. Transf. 25 (1981) 395.
[55] P.J. Leonard, Atom Data Nucl. Data Tables 14 (1976) 21.
[56] A. L'Huillier, L.A. Lompré, M. Ferray, X.F. Li, G. Mainfray, C. Manus, Europhys. Lett. 5 (1988) 601.
[57] A.E. Kingston, J. Opt. Soc. Am. 54 (1964) 1145.
[58] See http://www.crystran.co.uk/optical-materials/lithium-fluoride-lif.

[59] S. Duhm, A. Gerlach, I. Salzmann, B. Bröker, R.L. Johnson, F. Schreiber, N. Koch, Org. Electron. 9 (2008) 111.
[60] M.Z. Hasan, C.L. Kane, Rev. Mod. Phys. 82 (2010) 3045.
[61] D. Hsieh, D. Qian, L. Wray, Y. Xia, Y.S. Hor, R.J. Cava, M.Z. Hasan, Nature 452 (2008) 970.
[62] Y. Xia, D. Qian, D. Hsieh, L. Wray, A. Pal, H. Lin, A. Bansil, D. Grauer, Y.S. Hor, R.J. Cava, et al., Nat. Phys. 5 (2009) 398.
[63] M. Bianchi, D. Guan, S. Bao, J. Mi, B.B. Iversen, P.D.C. King, P. Hofmann, Nat. Commun. 1 (2010) 128.
[64] G.A. Burdick, Phys. Rev. 129 (1963) 138.
[65] See http://refractiveindex.info/?shelf=main&book=LiF&page=Li.
[66] See http://refractiveindex.info/?shelf=main&book=MgF2&page=Li-o.
[67] R. Mahon, T.J.M. Ilrath, V.P. Myerscough, D.W. Koopman, IEEE J. Quantum Electron. 15 (1979) 444.
[68] M.-C. Chen, M.R. Gerrity, S. Backus, T. Popmintchev, X. Zhou, P. Arpin, X. Zhang, H.C. Kapteyn, M.M. Murnane, Opt. Express 17 (2009) 17376.
[69] M. Chini, X. Wang, Y. Cheng, H. Wang, Y. Wu, E. Cunningham, P.-C. Li, J. Heslar, D.A. Telnov, S.-I. Chu, et al., Nat. Photon. 8 (2014) 437.
[70] S. Hädrich, A. Klenke, A. Hoffmann, T. Eidam, T. Gottschall, J. Rothhardt, J. Limpert, A. Tünnermann, Opt. Lett. 38 (2013) 3866.
[71] S. Hädrich, A. Klenke, J. Rothhardt, M. Krebs, A. Hoffmann, O. Pronin, V. Pervak, J. Limpert, A. Tünnermann, Nat. Photon. 8 (2014) 780.
[72] C.M. Heyl, J. Güdde, A. L'Huillier, U. Höfer, J. Phys. B: At. Mol. Opt. Phys. 45 (2012) 074020.
[73] F. Lindner, W. Stremme, M.G. Schätzel, F. Grasbon, G.G. Paulus, H. Walther, R. Hartmann, L. Strüder, Phys. Rev. A 68 (2003) 013814.
[74] E. Lorek, E.W. Larsen, C.M. Heyl, S. Carlström, D. Palecek, D. Zigmantas, J. Mauritsson, Rev. Sci. Instrum. 85 (2014) 123106.
[75] I. Pupeza, S. Holzberger, T. Eidam, H. Carstens, D. Esser, J. Weitenberg, P. Rußbüldt, J. Rauschenberger, J. Limpert, T. Udem, et al., Nat. Photon. 7 (2013) 608.
[76] M. Puppin, Y. Deng, O. Prochnow, J. Ahrens, T. Binhammer, U. Morgner, M. Krenz, M. Wolf, R. Ernstorfer, Opt. Express 23 (2015) 1491.
[77] J. Rothhardt, S. Hädrich, A. Klenke, S. Demmler, A. Hoffmann, T. Gotschall, T. Eidam, M. Krebs, J. Limpert, A. Tünnermann, Opt. Lett. 39 (2014) 5224.
[78] H. Wang, Y. Xu, S. Ulonska, J.S. Robinson, P. Ranitovic, R.A. Kaindl, Nat. Commun. 6 (2015) 7459.
[79] H. Bromberger, A. Ermolov, F. Belli, H. Liu, F. Calegari, M. Chávez-Cervantes, M.T. Li, C.T. Lin, A. Abdolvand, P.S.J. Russell, et al., Appl. Phys. Lett. 107 (2015) 091101.
[80] C.-T. Chiang, A. Blättermann, M. Huth, J. Kirschner, W. Widdra, Appl. Phys. Lett. 101 (2012) 071116.
[81] C.-T. Chiang, M. Huth, A. Trützschler, M. Kiel, F.O. Schumann, J. Kirschner, W. Widdra, New J. Phys. 17 (2015) 013035.
[82] C.-T. Chiang, M. Huth, A. Trützschler, F.O. Schumann, J. Kirschner, W. Widdra, J. Electr. Spectrosc. Relat. Phenom. 200 (2015) 15.